Combination of techniques to quantify the distribution of bacteria in their soil microhabitats at different spatial scales

Archana Juyal
Wilfred Otten
Ruth Falconer
Simona Hapca
Hannes Schmidt
Philippe C. Baveye
Thilo Eickhorst

This is the accepted refereed manuscript of:
Juyal A, Otten W, Falconer R, Hapca S, Schmidt H, Baveye PC & Eickhorst T (2019) Combination of techniques to quantify the distribution of bacteria in their soil microhabitats at different spatial scales. *Geoderma*, 334, pp. 165-174

The published article is available from doi:
https://doi.org/10.1016/j.geoderma.2018.07.031

Combination of techniques to quantify the distribution of bacteria in their soil microhabitats at different spatial scales

A. Juyal [a, b], W. Otten [a, c], R. Falconer [a], S. Hapca [a, d], H. Schmidt [b, e], P. Baveye [f], T. Eickhorst [b *]

[a] School of Science Engineering and Technology, Abertay University, Dundee, UK

[b] FB 2 (Biology/Chemistry), University of Bremen, Bremen, Germany

[c] School of Water, Energy and Environment, Cranfield University, Cranfield, UK

[d] School of Medicine, University of Dundee, Dundee, UK

[e] Department of Microbiology and Ecosystem Science, University of Vienna, Vienna, Austria

[f] AgroParisTech, Université Paris-Saclay, Thiverval-Grignon, France

* eickhorst@uni-bremen.de

Abstract

To address a number of issues of great societal concern at the moment, like the sequestration of carbon, information is direly needed about interactions between soil architecture and microbial dynamics. Unfortunately, soils are extremely complex, heterogeneous systems comprising highly variable and dynamic micro-habitats that have significant impacts on the growth and activity of inhabiting microbiota. Data remain scarce on the influence of soil physical parameters characterizing the pore space on the distribution and diversity of bacteria. In this context, the objective of the research described in this article was to develop a method where X-ray microtomography, to characterize the soil architecture, is combined with fluorescence microscopy to visualize

and quantify bacterial distributions in resin-impregnated soil sections. The influence of pore geometry (at a resolution of 13.4 µm) on the distribution of *Pseudomonas fluorescens* was analysed at macro- (5.2 mm x 5.2 mm), meso- (1 mm x 1 mm) and microscales (0.2 mm x 0.2 mm) based on an experimental setup simulating different soil architectures. The cell density of *P. fluorescens* was 5.59E+07 (s.e 2.6E+06) cells g^{-1} soil in 1-2 mm and 5.84E+07 (s.e 2.4E+06) cells g^{-1} in 2-4 mm size aggregates soil. Solid-pore interfaces influenced bacterial distribution at micro- and macroscale, whereas the effect of soil porosity on bacterial distribution varied according to three observation scales in different soil architectures. The influence of soil porosity on the distribution of bacteria in different soil architectures was observed mainly at the macroscale, relative to micro- and mesoscales. Experimental data suggest that the effect of pore geometry on the distribution of bacteria varied with the spatial scale, thus highlighting the need to consider an "appropriate spatial scale" to understand the factors that regulate the distribution of microbial communities in soils. The results obtained to date also indicate that the proposed method is a significant step towards a full mechanistic understanding of microbial dynamics in structured soils.

Keywords

X-ray CT; fluorescence microscopy; soil bacteria; pore geometry; soil sections; spatial distribution

1 Introduction

Soil microorganisms play a vital role in soil ecosystem processes, and their location is restricted to the conditions provided by microhabitats, whose properties vary, among other factors, due to the large spatial heterogeneity of soils (Vos et al., 2013). Bacteria tend to aggregate in their habitats and form what has been referred to as “microbial hotspots”. Hotspots are zones in which the biological activity is much faster and intensive compared to average soil conditions (Kuzyakov & Blagodatskaya, 2015). However, little is known about what controls the spatial distribution of bacteria in soil. Studying the spatial patterns at the microscale could help to determine the factors controlling microbial community and activity. Subsequently, this data and knowledge of the relevant factors could help in the development of predictive models that would foster the understanding of bacterial contributions to soil functions.

Over the years, the spatial distribution of indigenous and introduced bacteria has been studied in undisturbed or repacked soil columns, however the relationship between the bacterial spatial distribution and 3D soil architecture has not been considered (Nunan et al., 2001; Kizungu et al., 2001; Nunan et al., 2003; Dechesne et al., 2003; Pallud et al., 2004; Dechesne et al., 2005). Spatial isolation, afforded by the complexity of soil air-solid interfaces, is believed to be one of the key factors accounting for the diverse microbial communities in soils. Geometrical characteristics of the soil pore space, such as pore volume, shape, connectivity, size, and tortuosity of pathways can have an impact on microbial composition and activity in soil. They regulate the accessibility of organic matter, the diffusion of oxygen through the gaseous phase, and the diffusion of dissolved compounds through the water phase, as well as the movement of

69 microorganisms. These pore characteristics can be measured experimentally or can be
70 estimated via non-destructive imaging.
71 Advances in the application of X-ray micro-tomography have made it possible to
72 visualize and quantify the internal architecture of soils in three dimensions at µm
73 resolution. Recent studies (Kravchenko et al., 2013; Juarez et al., 2013; Wang et al.,
74 2013; Kravchenko et al., 2014; Negassa et al., 2015) have combined X-ray tomography
75 with other analytical methods to investigate the influence of pore geometry on
76 distribution (Kravchenko et al., 2013; Wang et al., 2013), composition (Ruamps et al.,
77 2011; Kravchenko et al., 2014), and activity (Ruamps et al., 2013; Juarez et al., 2013) of
78 bacterial communities in soil. These studies show how the combination of advanced
79 techniques can help in obtaining experimental evidence on relationships existing
80 between microbes and physical microscale environments. Whereas the results suggest
81 that the study of bacteria at a scale relevant to microorganisms is important, there is no
82 clarity yet what scale that should be and if relationships and observations differ across
83 scales.
84 In this general context, the aim of this article is to develop a procedure that can be used
85 to quantify the influence of pore geometry on the spatial distribution of bacteria in soil.
86 This was achieved by integrating 2-D fluorescence microscopy with 3-D X-ray
87 tomography techniques. The specific objectives of this study are (i) to quantify using X-
88 ray micro-tomography, the pore geometry of resin-impregnated soil microcosms
89 representing different soil architectures (aggregate sizes); (ii) to quantify bacterial
90 distributions in polished sections of resin-impregnated soils; and (iii) to determine if
91 there is an effect of the scale of observation, by analyzing the influence of pore

geometry on the distribution of introduced bacteria, through co-locating 2-D thin sections within a 3-D X-ray CT volume.

2 Materials and Methods

2.1 Preparation of soil microcosms

A sandy loam soil was collected from an experimental site, Bullion Field, situated at the James Hutton Institute, in Dundee, Scotland. The soil (5.4% SOM, C/N: 16.4, pH ($CaCl_2$): 6.1, electrical conductivity: 49 µS cm^{-1}) was dry-sieved and sterilized by autoclaving twice at 121°C and 100 kPa for 20 minutes with a 24 h interval time. Sieved aggregates of 1-2 mm and 2-4 mm size of this soil were used to prepare microcosms. These microcosms consisted of soil aggregates, packed in steel rings (16 mm inner diameter and 17 mm height, 3.4 cm^3 volume) at a defined bulk-density of 1.3 g cm^{-3}, and watered to reach a state with 40% water-filled pores. The moisture content was adjusted to 0.15 cm^3 g^{-1} by adding sterilised dH_20_{MQ} 48 h prior to packing. In each microcosm, 5.09 g of soil aggregates was inoculated with 500 µL of the bacterial suspension, mixed well to ensure an even distribution of the bacterial inoculum, and packed using a pushing rod. Control samples were packed in a similar manner except that sterile dH_20_{MQ} was used instead of the cell suspension. Three replicates per treatment for each sampling day were prepared, and the microcosms were sampled destructively four times.

To obtain the inoculum, an overnight culture of *Pseudomonas fluorescens* SBW25 was prepared in King's B medium at 23°C in the dark, washed in 1×PBS and adjusted to a specific cell density prior to inoculation using a spectrophotometer reading at

OD 600 nm (Thermo Fisher Scientific, UK). The cell density of *P. fluorescens* was 3.6E+07 cells mL^{-1} and thus 1.8E+07 cells were inoculated per microcosm. Additional samples were amended with 500 µL dH_20_{MQ} instead of inoculum serving as control treatments. Three replicates per treatment were prepared and sealed in plastic bags to avoid drying of samples. The samples were incubated at 23°C in the dark for 5 days to allow bacterial growth and spread through the soil. The soil microcosms were sampled after five days for resin impregnation, as explained in the next section.

2.2 Fixation and dehydration of soil microcosms

Soil microcosms were first placed onto a hardboard covered with layers of cotton mesh to prevent loss of soil during the embedding processes. Microcosms were then placed on top of an aluminium gauze stand in a container to support the subsequent steps required for fixation and resin impregnation. To preserve the distribution of bacteria within the soil matrix, the microcosms were fixed using a 2% formaldehyde solution (v/v in H_2O; 37% stock solution, Sigma Aldrich). This solution was added slowly from the sides of the container, to minimize disturbance of soil microcosms and facilitate the exchange of liquids (from bottom to top). All microcosms were completely submerged in the solution and kept overnight for fixation at 4°C. Subsequently, samples were washed in MQ distilled water for two hours, which was added the same way as the fixation solution. After washing, the samples were dehydrated with a graded series of acetone solutions (technical grade, VWR) to avoid interference with the polymerization of resin. Samples were submerged in 50% (v/v) acetone-water solution at room temperature for at least 12 hours. Subsequently a graded series of 70%, 90% and three times 100%

(v/v; acetone in water) was applied, each step lasting for 2 h. During the last two steps with 100% acetone, samples were kept under vacuum (280 mbar) to facilitate the complete exchange of all pores.

2.3 Resin impregnation of soil microcosms

A 2 L volume of impregnation mixture was prepared for a subset of up to 9 microcosms by adding 1300 µL of accelerator (0.95 ‰ (v/v) 1%-Cobalt Octoate accelerator, Oldopal, Büfa, Germany) and 2600 µL of hardener (1.9 ‰ (v/v) cyclohexanone peroxide, Akzo Nobel, Germany) to 1.4 L of polyester resin (Oldopol P50-01, Büfa, Germany), and 600 mL of acetone added as a thinner. The resulting mixture was mixed well and was kept under vacuum (240 mbar) to remove gas bubbles, until it was added to the samples.

Acetone was evacuated from the container with the soil samples, and the latter were then placed into a desiccator equipped with a tube and valve connected to the resin mixture container. Resin was then added drop by drop under vacuum (240 mbar, with the drops placed immediately next to the microcosms to allow an infiltration with resin from the bottom to the top to ensure that the pores of the soils were filled with resin mixture as completely as possible. Shortly before reaching the surface of the microcosms (after approx. 40 min) the addition of resin was stopped for a while and vacuum was increased (200 mbar) for 1 h. Finally, the remaining mixture was added to cover the sample completely with resin. Samples were left at room temperature under a hood for polymerization of the resin, which lasted 7 weeks. Resin impregnated samples were then cut, removed from steel rings, and the bottom and top were parallel ground on a cup wheel grinding machine (MPS2 120, G&N, Germany). Finally, a vertical cut

was made through the microcosm to ensure a proper orientation of each block during CT scanning and subsequent fluorescence microscopy.

2.4 X-ray CT of resin impregnated samples

The physical structure of resin-impregnated microcosms was obtained via X-ray µ-CT scanning (HMX ST 225, Metris X-Tek, UK) at a resolution of 13.4 µm per voxel. In order to visualize resin-filled pore space, samples were scanned under energy settings of 145 keV and 35 µA and 2000 angular projections. A molybdenum target and a 0.25 mm aluminium filter were used. Radiographs were reconstructed via software (CT Pro v.2.1, NIKON metrology, UK) into 3D volume datasets, which were adjusted in contrast and exported as image stacks (*.bmp format) via volume processing software (VGStudio Max 2.2, Volume Graphics, Germany).

2.5 Preparation of polished sections for cell counting

After CT scanning, polished sections were prepared for cell counting at three depths of each resin-impregnated microcosm (Supplementary Figure S1). To obtain these sections, blocks were first cut with a diamond saw (Woco 50, Conrad, Germany), then ground down to the estimated height (centre of the block and ±2.5 mm above and below the centre) using a cup wheel grinding machine (see above). Each ground surface was subsequently polished using wet abrasive paper on a glass plate (silicon carbide, P1200) to remove grinding material and make the surface smooth. The blocks were then cleaned with cleaning solvent and exact heights were measured using a micrometre (accuracy 1 µm).

184

185 *2.6 Alignment of polished sections and image processing*

186 A stereomicroscopic image of each polished section representing an individual layer of
187 resin impregnated microcosm was taken and used to find the corresponding layer in the
188 image stack of CT data (Supplementary Figure S2 (A, B)).Image stacks were rotated to
189 match the orientation of the stereo microscopic images, which corresponded to the
190 orientation of the virtual counting grid applied in cell counting. The selected CT image
191 was then cropped to the region of interest (where bacterial cells were counted) in Image
192 J v1.47 (http://rsbweb.nih.gov/ij/) (Supplementary Figure S2 (C)). The cropped region of
193 interest was then thresholded using the indicator kriging segmentation method (Houston
194 et al., 2013).

195

196 *2.7 Analysis of pore geometry*

197 The pore architecture of each microcosm was analysed at three different scales in 2D,
198 hereafter referred to as microscale, mesoscale, and macroscale. The areas selected for
199 the analysis of pore characteristics at each scale in individual microcosms are depicted
200 in Fig. 1. The microscale corresponds to each field of view of size 0.2 × 0.2 mm, the
201 mesoscale is associated with a field of view of size 1.0 × 1.0 mm, and finally the
202 macroscale encompasses the region of interest of size 5.2 × 5.2 mm (Fig.1). In 2D,
203 each slice was analysed with a thickness of one voxel.

204 Pore geometry was also analysed at the macroscale in 3D to get a broader perspective
205 on the relationship between pores and bacteria. For this, the neighbouring 476 slices,
206 above and below the plane, were used to calculate a measure of pore geometry in 3D.

207 The size of the area analysed at each scale is described in Table 1. A macro was
208 recorded in ImageJ v1.47 (hhtp://rsbweb.nih.giv/ij/) to crop images at the different
209 scales analysed. The segmented images were then evaluated by software developed
210 in-house (Houston et al., 2013a). This software was used to quantify pore
211 characteristics, like porosity, connectivity, and the area of solid-pore interfaces of the
212 pore volume, based on voxel data obtained from CT-scans. The porosity was calculated
213 as the volume fraction occupied by pores, whereas connectivity was determined as the
214 volume fraction of pore space that is connected with the external surface of the image
215 volume. The surface area of solid-pore interfaces was estimated using Minkowski
216 functionals, and expressed in relation to the area of solids directly connected to the pore
217 space (Houston et al., 2013b).
218
219 *2.8 Enumeration of bacteria in polished sections*
220 To enumerate bacteria, a drop of an anti-fading medium containing 1.5 µg mL^{-1} DAPI
221 stain (Vectashield H-1200, Vector Laboratories, USA) was applied on top of the
222 polished surface of blocks, which was covered afterwards with a cover slip (24 × 32
223 mm, Menzel Gläser, Germany). Bacterial cells were evaluated with a fluorescence
224 microscope (Axioscop 2, Carl Zeiss, Germany) equipped with an Hg vapour lamp (HBO
225 103 W/2, Osram, Germany) using a 63× objective lens (Plan-Neofluar, Carl Zeiss,
226 Germany). DAPI-stained cells were detected with an appropriate fluorescence filter set
227 (F46-000, AHF, Germany) and counted manually using an ocular with an integrated
228 squared grid reticle (10 × 10, 1.25 mm^2; Carl Zeiss, Germany). Cell counts were
229 obtained at counting spots arranged on a grid of 6 × 6 fields of view with distance of 1

mm in x- and y-direction respectively resulting in a total area of 5.2 × 5.2 mm per polished section (Fig. 1). The location of the starting point for each analysed layer was chosen by placing each polished block on a reference slide and following the coordinate system on the microscopic stage. Thus, the same position of the virtual counting grid could be applied for each block and layer. Cell counts were extrapolated from cell counts per area of field of view to cells per gram of dry soil by assuming a focus depth of 4 µm during fluorescence microscopic observation.

2.9 Statistical analysis

Statistical analysis was performed using SPSS software version 21. A mixed effect linear model (assuming normal distribution) was applied to investigate differences in soil pore characteristics between treatments, with treatments as fixed factor and three individual microcosms per treatment as error term for treatment. To comply with the normality assumption, the porosity and connectivity measures were transformed using the probit function. Data relative to the solid-pore interfacial area met the normality assumption.

A generalized mixed-effect Poisson model with log-link function was used to investigate significant differences in cell numbers between different treatments, with treatment taken as a fixed factor. The effect of soil pore characteristics such as porosity, connectivity, and solid-pore interfacial area, on the distribution of bacteria was also determined by a Poisson model with treatment as a fixed factor. The size of the analysed scale was introduced as an offset variable in the Poisson model.

253 ## 3 Results

254 ### *3.1 Pore geometry of resin impregnated soil*

255 Among the two different aggregate sizes, a distinguishable difference in visible soil
256 pores larger than minimum size of 13.4 µm was evident by visual inspection of the 2D
257 sliced images derived from the analysed layer (Fig. 2). An increase in the size of pores
258 with increasing diameter of aggregates was clearly visible. The visual difference was
259 however not apparent among the quantitative measures of the pore geometry analysed
260 at different scales.

261 The three studied scales differed in terms of porosity and solid-pore interface between
262 the two treatments. The average values of soil pore characteristics at different scale for
263 each treatment are presented in Table 2. In terms of porosity the samples analysed at
264 microscale were not significantly different ($p = 0.929$), with average porosity of 20.8% in
265 1-2 mm and 19.2% in 2-4 mm sized soil aggregates. The average solid-pore interfacial
266 area was slightly higher in 2-4 mm than in 1-2 mm aggregate size treatment (Table 2),
267 however the difference was not statistically significant ($p > 0.05$). In samples analysed
268 at mesoscale 2D, even though the average porosity was slightly higher in 2-4 mm
269 (21.5%) than in 1-2 mm (19.3%) aggregate soil (Table 2), the difference was not
270 statistically significant ($p > 0.05$). However, the average solid-pore interfacial area
271 between treatments was statistically significant ($p < 0.001$), with 0.036 mm^2 in 1-2 mm
272 and 0.041 mm^2 in 2-4 mm sized soil aggregates. At macroscale 2D, soil porosity was
273 very similar and not significantly different between the two treatments. The average
274 solid-pore interfacial area was higher in 2-4 mm (1.070 mm^2) than 1-2 mm (0.967 mm^2)
275 aggregate size treatment, however no significant difference ($p > 0.05$) was observed.

In samples analysed at the macroscale in 3D, even though the differences in average soil porosity between the two treatments was very minor, with average porosity of 20.9% in 1-2 mm and 20.0% in 2-4 mm sized soil aggregates, the difference was statistically significant ($p < 0.001$). Soil connectivity was also significantly different ($p < 0.001$) between treatments, with an average connectivity of 96.16% in 1-2 mm and 94.29% in 2-4 mm aggregate sized soil. However, the solid-pore interfacial area among different aggregate size treatments was not significantly different, with 8.05 mm^2 in 1-2 mm and 7.72 mm^2 in 2-4 mm aggregates sized soil ($p > 0.05$).

3.2 Visualisation and quantification of bacterial distribution in soil

Under UV excitation, bright blue signals of the stained *Pseudomonas* cells were detected on impregnated samples. Although soil particles and resin exhibited blue autofluorescence as well, the stained cells were easily distinguishable against the background (Supplementary Figure S3). DAPI-stained *Pseudomonas* cells appeared evenly spread mainly on the surface of the clay-humus complexes or at solid-pore interfaces. Very few (1-3) cells were observed in a resin-filled pore area surrounding the soil particles. No DAPI signals were detected in negative control samples of sterilized soils without inoculum. Visual comparison of cell density in each analysed layer of a treatment was carried out to determine treatment effects (Fig. 3). Cell density ranged from 25 to 700 cells per counting spot in the treatment with 1-2 mm aggregate sizes compare to 0 to 650 cells per counting spot in the treatment with aggregate size of 2-4 mm. In general, the cell numbers of both treatments differed between different counting spots on each analysed layer. Therefore, the result showed a variation in the number of

299 cell counts between different treatments. The cell density of *Pseudomonas* was 290.8
300 (s.e=13.4) cells mm^{-2} in 1-2 mm and 303.7 (s.e=12.7) cells mm^{-2} in 2-4 mm soil
301 aggregates. These numbers correspond to 5.59E+07 (s.e 2.6E+06) cells g^{-1} and
302 5.84E+07 (s.e 2.4E+06) cells g^{-1}, respectively, in columns packed with 1-2 mm and 2-4
303 mm soil aggregates.
304
305 *3.3 Influence of soil pore geometry on bacterial distribution at different scales*
306 To examine the relationship between soil pore geometry and bacterial cell counts, the
307 cell density (no. of cells mm^{-2}) of *Pseudomonas* was plotted against soil porosity and
308 solid-pore interfacial area analysed at different scales (Fig. 4, SI Fig. S4). In Figure 4,
309 more data points are plotted in the microscale and mesoscale graphs compared to the
310 macroscale graphs. This is because each data point in the graphs corresponds to the
311 analysis of a counting spot of individual layer in each replicate of a respective treatment.
312 Therefore, there is a noticeably wider spread in the cell density values in the graphs
313 showing data at the microscale and mesoscale, compared to the macroscale.
314 At microscale 2D, the values of the solid-pore interfacial area ranged from 0.000-0.008
315 mm^2 for the 1-2 mm aggregate size and 0.000-0.010 mm^2 for the aggregate size 2-4
316 mm. The cell density ranged between 0-1600 cells mm^{-2} (Fig. 4a & b). The influence of
317 soil porosity and solid-pore interfacial area on the distribution of *Pseudomonas* cells
318 varied between treatments (Table 3). At the microscale, the influence of soil porosity on
319 *Pseudomonas* cell distribution was statistically significant ($p = 0.001$), showing a slight
320 reduction ($\beta = - 0.0301$) in cell density with increasing porosity, for samples made up of
321 2-4 mm. No significant trend was found for samples with aggregates 1-2 mm., However,

322 the influence of solid-pore interfacial area on the distribution of *Pseudomonas* cells was
323 statistically significant in both aggregate size treatments (Table 3), but showed a
324 contrasting effect with a decrease for aggregates sized 1-2 mm (β = -19.203) and an
325 increase for aggregates sized 2-4 mm (β = 16.417) aggregates. In samples analysed at
326 the mesoscale in 2D, the solid-pore interfacial area ranged from 0.00-0.10 mm^2 for the
327 1-2 mm aggregate size and 0.00-0.012 mm^2 for 2-4 mm aggregates. The cell density
328 ranged between 0-1600 cells mm^{-2} (Fig. 4 c & d). Compared to the microscale, at the
329 mesoscale only soil porosity in samples made up of 1-2 mm aggregates significantly
330 influenced (p = 0.030) the distribution of bacterial cells, showing a small decrease (β = -
331 0.051) in the cell density with increasing porosity. For samples made up of 2-4 mm
332 aggregates, distribution of *Pseudomonas* cells was not significantly influenced by
333 porosity or the solid-pore interfacial area.
334 At the macroscale, cell density refers to the average of cell counts over 36 counting
335 spots in each analysed layer. For samples analysed at the macroscale in 2D, solid-pore
336 interfacial area ranged from 0.5-1.0 mm^2 in the 1-2 mm aggregate size and 0.5-2.5 mm^2
337 in the 2-4 mm sized aggregates. The mean cell density ranged from 0-500 cells mm^{-2}
338 (Fig. 4 e & f). The influence of soil porosity on *Pseudomonas* cell distribution was
339 statistically significant (p = 0.000) in both treatments, with a decrease (β = - 0.849 for 1-
340 2 mm and β= -0.794 for 2-4 mm) in cell density with increasing porosity. The influence
341 of solid-pore interfacial area also showed statistically significant influence on distribution
342 of *Pseudomonas* cells for both sized aggregates. In samples analysed at the
343 macroscale in 3D, between the two treatments the soil porosity of the analysed area
344 ranged from 10-30%, connectivity of pores ranged from 90-100% and solid-pore

345 interfacial area ranged from 1.2-2.5 mm^2 (Fig. 5). In both treatments, the distribution of
346 *Pseudomonas* cells was significantly influenced by porosity, connectivity, and solid-pore
347 interfacial area. However, these effects show contrasting influence when compared for
348 the two aggregate sizes. For aggregate size 1-2 mm, porosity, connectivity and soil-
349 pore interface have negative effect on the cell density. Whereas for aggregate size 2-4
350 mm, these three parameters show positive effect (Table 4).
351

352 ## 4 Discussion

353 ### *4.1 Bacterial distribution*

354 In this study bacteria were visualized with the intercalating DNA stain DAPI. This stain
355 has been used to visualize indigenous bacteria in resin-impregnated soil samples
356 before (Li et al., 2003; Eickhorst & Tippkötter, 2008), and as a counter-stain in
357 undisturbed soil samples (e.g., Eickhorst & Tippkötter, 2008). No DAPI signals were
358 detected in control samples, which confirms that the autoclaving procedure successfully
359 sterilized the soils and that the bacteria that are visualized in inoculated samples were
360 those introduced artificially. *Pseudomonas* cells were observed at solid-pore interfaces.
361 The very few cells observed in the pore space were most likely cells closely connected
362 to solid-pore interfaces above or below the targeted soil pore. This observation is no
363 surprise and is inherent to the impregnation method because if, as is likely based on
364 earlier experiments (Vandevivere and Baveye, 1992), there had been cells in the lumen
365 of pores, they would have been removed or forced onto the surfaces during the
366 exchange of liquids for the fixation and dehydration of the samples.

In order to investigate the impact of the different treatments during sample preparation (fixation, washing, and dehydration), a separate series of soil microcosms was tested for cell removal during these steps (Supplementary data S5). The results of this test showed that relative cell losses ranged from -1.26% after fixation to -0.25% after dehydration for *Pseudomonas* cells which is a negligible proportion and shows that the majority of bacteria were attached to the surfaces throughout the preparatory treatments. For non-autoclaved samples, relative cell losses were even lower (by approx. 100 times), suggesting that the observed cell losses during preparation are a result of the inoculation of cells in this experiment.

In polished sections, *Pseudomonas* cells were observed to be distributed as single cells through the soil matrix. White et al (1994) also observed a similar distribution of *Pseudomonas fluorescens* stained cells throughout the soil pore network. This kind of pattern was different than for indigenous bacteria that were observed in the form of small clusters or microcolonies constituted by cells of identical or different morphologies (Nunan et al., 2001; Li et al., 2004; Eickhorst & Tippkotter, 2008). Raynaud and Nunan (2014) also observed an aggregated pattern in distribution of indigenous bacteria in thin sections of soil. This suggests that the distribution of bacteria in soil is an effect of extrinsic (pore size and organic matter) and intrinsic (reproduction by binary fission) processes in soil. Differences in the distribution pattern can also be related to how bacteria spread and access nutrient sources in soil. A different response between species can be expected in their relationship with the soil architecture. In this study, although based on visual inspection, it seemed that the introduced bacteria were

389 homogenously mixed within the samples, a heterogeneous distribution in cell counts
390 between different counting spots was observed.
391 Dechesne et al. (2005) also showed that the distribution of introduced bacteria was
392 more heterogeneously distributed than that of indigenous bacteria. Other results have
393 also shown a non-random distribution of microorganisms in soil (Nunan et al., 2003;
394 O'Donnell et al., 2007; Young et al., 2008). We stress that although the technique we
395 develop here has generic validity, the specific interrelationships that are found between
396 aspects of pore geometry and bacterial distribution may therefore be a result of the
397 system we deployed. It is, for example, reasonable to expect that when bacteria are
398 randomly mixed with soil, as is the case in our experiments, time will need to elapse for
399 a different relationship to develop. When bacteria are mixed through soil, connectivity of
400 the pore space may not be a factor contributing to the distribution. However,
401 connectivity of pore space is required for bacteria to move through soil. The fact that we
402 still observe relationships in our results can be explained by the fact that *Pseudomonas*
403 is expected to spread over significant distances under these experimental conditions
404 (Juyal et al., 2018). In this study, Juyal a et al (2018) also showed that the rate of
405 growth depends on the soil structure. There is a complex number of factors influencing
406 bacterial distribution, ranging from physical (pore geometry), to nutritional and biological
407 factors (differences in motility and attachment). Some studies have related the variation
408 in bacterial distribution to a range of factors like organic matter content, soil moisture
409 content, aggregate size classes and their location within aggregate, and pore size class
410 (Franklin and Mills, 2009; Kravchenko et al., 2014; Or et al., 2007; Ruamps et al., 2011).
411 The dominant processes however remain to be identified, but the technique developed

here offers real opportunities to disentangle these processes as for the first time 2-D thin sections are placed within a 3-D geometry. Among different aggregate size treatments, a significant difference in *Pseudomonas* cell density was observed. Samples with 2-4 mm aggregate size had higher cell density compare to samples with 1-2 mm aggregate size. Similar kinds of differences in numbers of bacterial populations have been reported by past studies related to different soil particle sizes or aggregate fractions (Ranjard and Richaume, 2001; Sessitsch et al., 2001).

4.2 Influence of pore geometry on bacterial distribution

The key goal of this article was to develop a methodological approach to analyse the effect of pore characteristics on spatial patterns of bacteria at scales associated with microhabitats. The approach consists of combining 2D and 3D methods to gain quantitative information on the relationship between pore characteristics and bacteria introduced in soil. It is known from previous research that the spatial distribution of bacteria is not random at fine scales and their location in soil is dependent on factors like substrate availability, soil water, and pore size distribution (Nunan et al., 2003; Ruamps et al., 2011). Along the same lines as what we attempt in this article, Hapca et al. (2011, 2015) developed a statistical method to combine 2D SEM-EDX data with 3D X-ray tomography images to generate the 3D spatial distribution of chemical elements in soil. Progress has been made combining techniques to analyse the relationship between soil pore characteristics and microbial community distribution and their activity in soil. For example, Kravchenko et al. (2013) studied the effect of intra-aggregate pore geometry on the distribution of *E. coli* in macro-aggregates. They used culture-based

methods (colony forming unit method) to enumerate *E. coli* distribution in aggregates and X-ray tomography to quantify pore architecture of intact aggregates from different managements. In our study, microscopic examination of polished sections was used to quantify bacteria in soil. The advantage of this method used over the culture- and non-culture-based approaches is that the use of impregnated soil samples made it possible to characterize the *in situ* relationship between bacteria and soil features without destroying the samples. Another advantage of this methodology was the use of X-ray CT to quantify pore architecture in the same layer.

The relationship between pore geometry and bacterial cell density was analysed at different scales. The scale at which observations are made is often determined by technology alone, but here we quantified the effect of pore geometry at the scale at which microbes actually live and interact with their surrounding environment and also if the effect is specific to that scale or variable at large scales. From the published literature, it appears that opinions concerning what range of microscales needs to be considered depending upon the individual microorganism under study, the microbial process of interest, and also to some extent on the tools available for the studies (Grundmann, 2004). Therefore, the scales used in this study have been defined based on the appropriate scales of the applied techniques, i.e., computed tomography (macroscale in this study) and fluorescence microscopy (microscale in this study). Analysis at different scales has been carried out by others to study the spatial pattern of either indigenous bacterial population (Nunan et al. 2002) or microbial activity (Gonod, 2006) from meter to micro-meter scales. These authors identified spatial structures of bacterial populations at microscale in topsoils and at large and microscale in subsoils.

458 They related this difference in spatial pattern at different depths to transport of nutrients
459 through soil (Nunan et al., 2002). Therefore, it is noted that different significant effects
460 are found depending on the spatial scale of analysis. This confirms that the spatial scale
461 of observation is an important aspect to be considered when doing this type of analysis,
462 but it also raises the question of what might be causing this effect and how best to
463 proceed. Therefore, we need to fully understand the spatial variability of soil microbes at
464 different scales.
465 In this study, the analysis at each scale was done in 2D and 3D for two key reasons.
466 First, the connectivity of pores, which is an important parameter in relation to transport
467 of nutrients and bacteria cannot be determined in 2D, and second, the degree of
468 tortuosity of the pore space is different in 2D compared to 3D. In our experiments, no
469 significant difference in the pore characteristics in 2D and 3D between different
470 aggregate size treatments was observed, but it should be noted that a part of the pore
471 volume, associated with sub-resolution pores, could not be detected by the X-ray
472 scanner due to limitation of the scan resolution, which was selected so as to enable us
473 to scan entire microcosms. Therefore, the conclusions made here are based on the
474 proportion of pores actually observed (i.e., pores larger than CT-scan resolution of
475 >13.4 µm). This fact had an effect on the analysed solid-pore interfaces as well, where
476 many data points in the microscale and mesoscale data were observed at zero (Fig. 4).
477 The respective cell counts were observed on the portion of pore volume that was not
478 detected by X-ray CT. Despite this issue, an influence of pore characteristics on
479 *Pseudomonas* distribution at different spatial scales (macro-, meso- and microscale in

480 this case) was supported by the data. But the effect was quite variable across the three
481 scales analysed over different dimensions in each treatment.
482 Samples analysed in two dimensions (2D) at macroscale showed a significant effect of
483 porosity on *Pseudomonas* cell distributions in both treatments but at mesoscale and
484 microscale this was not the case as the solid-pore interface showed no significant effect
485 on the distribution of *Pseudomonas* cells in all treatments. This difference between the
486 two scales could be due to the size of the sample as the information is constrained at
487 this scale. Therefore, to avoid this problem of sample size used for pore soil architecture
488 determination, the analysis was done in 3D where a bit of the surrounding area of the
489 3D soil environment was considered. The results showed that at macroscale, all three
490 pore characteristics exhibited a significant effect on the *Pseudomonas*-inoculated
491 treatment. This difference in analysis between two dimensions could be that in 2D the
492 information of pore characteristics information is constrained to the 2D-single plane from
493 3-D pore geometry. The results show that there was no general relationship between
494 pore geometry and bacterial counts and this varied with the spatial scale and
495 dimension, therefore measuring and identifying whether a relationship exists are tightly
496 linked to identifying the 'appropriate spatial scale'. The appropriate scale is needed to
497 help understand the development of the microbial spatial patterns and to determine the
498 factors that regulate and maintain soil biodiversity and microbial community function in
499 soil. We advocate that the use of mechanistic models that include explicit description of
500 microbial dynamics and soil architecture, such as those developed by Portell et al.
501 (2018), will be required to advance our understanding of complex interrelationships at
502 these scales and will offer an evidence base for identification of the scale dependence

503 of relationships between soil structure and bacterial distribution. Data sets as provided
504 in this study will be imperative towards further development and testing of such models.
505
506
507 ## 5 Conclusion
508 In this paper, a methodology is presented to determine the effect of pore geometry on
509 the distribution of bacteria at a range of spatial scales. The data presented in this paper
510 suggest that porosity, connectivity, and solid-pore interfaces influence the distribution of
511 bacteria in soils at macroscales. The development of the method presented here is a
512 significant step towards understanding how bacterial distribution is affected by soil
513 architecture in various applications and experimental conditions (e.g., packed
514 microcosm systems or undisturbed natural soil samples). Our research also raises
515 several issues regarding the “appropriate” spatial scale at which to carry out analyses.
516 This question is crucial, and in the absence of a general trend, the scale containing the
517 most representative information, within practical limits, should be selected for further
518 analysis. For a combination of techniques this may require to sample at different spatial
519 scales. The information obtained using this approach can lead to new frameworks to
520 model the distribution of bacteria in a 3D soil environment, which in due course, should
521 result in more accurate predictions of, e.g., biophysical processes driving C dynamics in
522 a range of situations (e.g., Falconer et al., 2015; Portell et al., 2018).
523
524
525 **Acknowledgement**

We gratefully acknowledge the financial assistance of SORSAS and of the German Academic Exchange Service (DAAD), through a scholarship (A/12/76235) awarded to the first author. WO and SH also acknowledge support from NERC (NE/H01263X/1 and NE/P014208/1). TE received funding from the University of Bremen (ZF/02/600/10). The underlying data can be accessed through the Cranfield University data repository at http://doi.org/10.17862/cranfield.rd.6860717

References

Dechesne, A., Pallud, C. Debouzie, D. Flandrois, J.P. Vogel, T.M. Gaudet, J.P. and Grundmann, G.L. 2003. A novel method for characterizing the microscale 3D spatial distribution of bacteria in soil. *Soil Biology and Biochemistry*. 35(12): pp. 1537–1546.

Dechesne, A., Bertolla, F. Grundmann, L. Lyon, C.B. and Icrobiol, APPLE N. M. 2005. Impact of the microscale distribution of a *Pseudomonas* strain introduced into soil on potential contacts with indigenous bacteria. *Applied And Environmental Microbiology*. 71(12): pp. 8123–8131.

Eickhorst, T., and Tippkotter, R. 2008. Detection of microorganisms in undisturbed soil by combining fluorescence in situ hybridization (FISH) and micropedological methods. *Soil Biology and Biochemistry*. 40(6): pp. 1284–1293.

547 Falconer, R., Battaia, G. Schmidt, S. Baveye, P. Chenu, C. and Otten, W. 2015.
548 Microscale heterogeneity explains experimental variability and non-linearity in soil
549 organic matter mineralisation. *PloS one*. 10(5): e0123774.
550 Hapca, S. M., Wang, Z. X., Otten, W., Wilson, C., and Baveye, P. C. 2011. Automated
551 statistical method to align 2D chemical maps with 3D X-ray computed micro-
552 tomographic images of soils. *Geoderma, 164*(3-4), 146-154.
553 doi:10.1016/j.geoderma.2011.05.018
554 Hapca, S.M., Baveye, P.C. Wilson, C. Lark, R.M. and Otten, W. 2015. Three-
555 dimensional mapping of soil chemical characteristics at micrometric scale by
556 combining 2D SEM-EDX data and 3D X-ray CT images. *PloS One.* 10(9):
557 e0137205.
558 Houston, A.N., Otten, W. Baveye, P.C. and Hapca, S. 2013a. Adaptive-window indicator
559 kriging: A thresholding method for computed tomography images of porous media.
560 *Computers & Geosciences*. 54: pp. 239–248.
561 Houston, A.N., Schmidt, S. Tarquis, A.M. Otten, W. Baveye, P.C. and Hapca, S. 2013b.
562 Effect of scanning and image reconstruction settings in X-ray computed
563 microtomography on quality and segmentation of 3D soil images. Geoderma. 207:
564 pp.154-165.
565 Juarez, S., Nunan, N. Duday, A-C. Pouteau, V. Schmidt, S. Hapca, S. Falconer, R.
566 Otten, W. and Chenu, C. 2013. Effects of different soil structures on the
567 decomposition of native and added organic carbon. *European Journal of Soil*
568 *Biology*. 58(September 2013): pp. 81–90.

569 Juyal A, Eickhorst T, Falconer R, Baveye PC, Spiers A and Otten W. (2018). Control of
570 Pore Geometry in soil Microcosms and Its effect on the growth and spread of
571 *Pseudomonas* and *Bacillus sp*. Front. Environ. Sci. 6:73. doi:
572 10.3389/fenvs.2018.00073
573 Kizungu, R., Grundmann, G.L. Dechesne, A. Bartoli, F. Flandrois, J.P. and Chasse, J.L.
574 2001. Spatial modeling of nitrifier microhabitats in soil. *Soil Science Society of*
575 *America Journal*. 1709: pp. 1709–1716.
576 Kravchenko, A. Chun, H-C. Mazer, M. Wang, W. Rose, J.B. Smucker, A. and Rivers, M.
577 2013. Relationships between intra-aggregate pore structures and distributions of
578 Escherichia coli within soil macro-aggregates. *Applied Soil Ecology*. 63: pp. 134–
579 142.
580 Kravchenko, A.N., Negassa, W.C. Guber, A.K. Hildebrandt, B. Marsh, T.L. and Rivers,
581 M.L. 2014. Intra-aggregate pore structure influences phylogenetic composition of
582 bacterial community in macroaggregates. *Soil Science Society of America Journal*.
583 78(6): pp. 1924-1939.
584 Kuzyakov, Y., and Blagodatskaya, E. 2015. Microbial hotspots and hot moments in soil:
585 concept & review. *Soil Biology and Biochemistry*. 83(2015): pp. 184–199.
586 Li, Y., Dick, W.A. and Tuovinen, O.H. 2003. Evaluation of fluorochromes for imaging
587 bacteria in soil. *Soil Biology and Biochemistry*. 35(6): pp. 737–744.
588 Li, Y., Dick, W.A. and Tuovinen, O.H. 2004. Fluorescence microscopy for visualization
589 of soil microorganisms: a review. *Biology and Fertility of Soils*. 39(5): pp. 301–311.
590 Negassa, W.C., Guber, A.K. Kravchenko, A.N. Marsh, T.L. Hildebrandt, B. and Rivers,
591 M.L. 2015. Properties of soil pore space regulate pathways of plant residue

592 decomposition and community structure of associated bacteria. *PloS one*. 10(4): p.
593 e0123999.
594 Nunan, N., Ritz, K. Crabb, D. Harris, K. Wu, K. Crawford, J.W. and Young, I.M. 2001.
595 Quantification of the in situ distribution of soil bacteria by large-scale imaging of thin
596 sections of undisturbed soil. *FEMS Microbiology Ecology*. 36: pp. 67–77.
597 Nunan, N., Wu, K. Young, I.M. Crawford, J.W. and Ritz, K. 2002. In situ spatial patterns
598 of soil bacterial populations, mapped at multiple scales, in an arable soil. *Microbial*
599 *Ecology*. 44(4): pp. 296–305.
600 Nunan, N., Wu, K. Young, I.M. Crawford, J.W. and Ritz, K. 2003. Spatial distribution of
601 bacterial communities and their relationships with the micro-architecture of soil.
602 *FEMS Microbiology Ecology*. 44(2): pp. 203–15.
603 O'Donnell, A.G., Young, I.M. Rushton, S.P. Shirley, M.D. and Crawford, J.W. 2007.
604 Visualization, modelling and prediction in soil microbiology. *Nature reviews.*
605 *Microbiology*, 5(9): pp. 689–99.
606 Or, D., Smets, B.F. Wraith, J.M. Dechesne, A. and Friedman, S.P. 2007. Physical
607 constraints affecting bacterial habitats and activity in unsaturated porous media–a
608 review. *Advances in Water Resources*.*30*(6): pp. 1505-1527.
609 Pallud, C., Dechesne, A. Gaudet, J.P. Debouzie, D. Grundmann, G.L. Lyon, B. Cedex,
610 V. and Lyon, C.B. 2004, Modification of spatial distribution of 2, 4-
611 dichlorophenoxyacetic acid degrader microhabitats during growth in soil columns.
612 *Applied and Environmental Microbiology*. 70(5): pp. 2709–2716.
613 Portell X, Pot V, Garnier P, Otten W and Baveye, PC. (2018). Microscale heterogeneity
614 of the spatial distribution of organic matter can promote bacterial biodiversity in

soils: insights from computer simulations. Front. Microbiol. 9:1583. doi: 10.3389/fmicb.2018.01583

Ranjard, L., and Richaume, A. 2001. Quantitative and qualitative microscale distribution of bacteria in soil. *Research in Microbiology*.152(8): pp. 707-716.

Ruamps, L.S., Nunan, N. and Chenu, C. 2011. Microbial biogeography at the soil pore scale. *Soil Biology and Biochemistry*. 43(2): pp. 280–286.

Ruamps, L.S., Nunan, N. Pouteau, V. Leloup, J. Raynaud, X. Roy, V. and Chenu, C. 2013. Regulation of soil organic C mineralisation at the pore scale. *FEMS Microbiology Ecology*. 86(1): pp. 26–35.

Raynaud, X., and Nunan, N., 2014. Spatial ecology of bacteria at the microscale in soil. *PLoS One*,*9*(1): p.e. 87217.

Sessitsch, A., Weilharter, A. Gerzabek, M.H. Kirchmann, H. and Kandeler, E. 2001. Microbial population structures in soil particle size fractions of a long-term fertilizer field experiment.*Applied and Environmental Microbiology*.67(9): pp. 4215-4224.

Vandevivere, P., & Baveye, P. 1992. Saturated hydraulic conductivity reduction caused by aerobic bacteria in sand columns. *Soil Science Society of America Journal. 56*(1): pp. 1-13.

Vos, M., Wolf, A.B. Jennings, S.J. and Kowalchuk, G.A. 2013. Micro-scale determinants of bacterial diversity in soil. *FEMS Microbiology Reviews*. 37(6): pp. 936–54.

Wang, Y., Bradford, S.A. and Simunek, J. 2013. Transport and fate of microorganisms in soils with preferential flow under different solution chemistry conditions. *Water Resources Research*. 49(5): pp. 2424–2436.

637 White, D., Fitzpatrick, E.A. and Killham, K. 1994. Use of stained bacterial inocula to
638 assess spatial distribution after introduction into soil. *Geoderma*. 63(3-4): pp. 245–
639 254.
640 Young, I., Crawford, J. and Nunan, N. 2008. Microbial distribution in soils: Physics and
641 scaling. *Advances in Agronomy*. 100: pp. 81-121.
642

Figure captions

Figure 1

Diagrammatic representation of spots where bacterial cells were counted in the given area of interest under the fluorescent microscope. Top row: greyscale images after CT-scanning for each scale (left: macroscale, centre: mesoscale, right: microscale; resolution: 13.4 µm). Bottom row: corresponding thresholded images. The grey squares in the bottom row represent each counting spot of size 0.2 x 0.2 mm. The distance between each counting spot was set to 1 mm. Grid in the microscale image (bottom right) represents the raticle grid used for cell enumeration in a single field of view.

Figure 2

Visual comparison of grey scale (left) and thresholded (right) images of the physical structure of soil with aggregate size 1-2 mm (A) and 2-4 mm (B).

Figure 3

Visual comparison of two-dimensional stereomicroscope images (left) and cell counts (right). One analysed layer is exemplarily shown for each treatment; (A) *Pseudomonas fluorescens* inoculated in packed 1-2 mm soil aggregates and (B) *Pseudomonas fluorescens* inoculated in packed 2-4 mm soil aggregates.

Figure 4

Relationship between bacteria cell density and soil-pore interface at microscale (A, B), mesoscale (C, D) and macroscale (E, F) in 2D in soil with aggregates of size 1-2 mm (left column; A, C, E) and 2-4 mm (right column; B, D, F). Data points in the graph represent individual counting spots per treatment (microscale and mesoscale) and means of each layer per treatment (macroscale; ±SE, *n*=3).

Figure 5

Relationship between mean bacteria cell density and porosity, connectivity and soil-pore interface at macroscale in 3D in soil with aggregates of size 1-2 mm (white dots) and 2-4 mm (grey dots). Data points in the graph represent individual analysed volumes of each replicate per treatment. Data are means ±SE (*n*=3).

Tables

Table 1

Physical dimensions of the region of interest (ROI) analysed for pore structure at macroscale, mesoscale, and microscale in 2D and 3D.

Scales	Dimensions	Physical dimension of ROI	
		(mm)	(voxel)
Microscale	2D	0.2 × 0.2	15 × 15
Mesoscale	2D	1.0 × 1.0	77 × 77
Macroscale	2D	5.2 ×5.2	400 × 400
	3D	6.2 × 6.2 × 6.2	476 × 476 × 476

Table 2

Average values of soil porosity and soil-pore interface analysed at macroscale, mesoscale and microscale in 2D. Mean cell counts ±SE are presented. Superscript letters indicate significant differences between aggregate size and scales ($p < 0.01$).

Scale	*n*	Porosity (%)		Soil-pore interface (mm²)	
		1-2 mm aggregates	2-4 mm aggregates	1-2 mm aggregates	2-4 mm aggregates
Microscale 2D	364	20.82 ± 1.86 [a]	19.26 ± 1.78 [a]	0.001 ± 0.000 [a]	0.002 ± 0.000 [a]
Mesoscale 2D	364	19.37 ± 0.96 [a]	21.50 ± 1.11 [a]	0.036 ± 0.001 [b]	0.041 ± 0.001 [b]
Macroscale 2D	9	21.05± 2.28 [a]	21.08 ± 2.21 [a]	0.967 ± 0.038 [c]	1.070 ± 0.097 [c]

48 **Table 3**

49 Results of the Poisson model analysis on influence of pore structure on distribution of
50 bacteria in soil with different aggregate sizes at microscale, mesoscale, and macroscale
51 in 2D. Numbers reported in the table are the p-values and coefficient values (*β*) are the
52 estimation of the fixed coefficients (porosity and soil-pore interface) in the test model of
53 the analysis.

Scales	Treatments	Porosity		Soil-pore interface	
		p-value	Coefficient *β*	p-value	Coefficient *β*
Microscale 2D	*Pseudomonas* inoculated in soil with aggregate sizes 1-2 mm	0.469	0.006	0.027	-19.203
	Pseudomonas inoculated in soil with aggregate sizes 2-4 mm	0.001	-0.0301	0.025	16.417
Mesoscale 2D	*Pseudomonas* inoculated in soil with aggregate sizes 1-2 mm	0.030	-0.051	0.297	0.962
	Pseudomonas inoculated in soil with aggregate sizes 2-4 mm	0.609	-0.009	0.187	-0.931
Macroscale 2D	*Pseudomonas* inoculated in soil with aggregates sizes 1-2 mm	0.000	-0.849	0.025	-0.536
	Pseudomonas inoculated in soil with aggregate sizes 2-4 mm	0.000	-0.794	0.001	-1.439

54

55

Table 4

Results of the Poisson model analysis on influence of pore structure on distribution of bacteria in soil with different aggregate size at macroscale in 3D. Numbers reported in the table are the p-values and coefficient values (*β*) are the estimation of the fixed coefficients (porosity and soil-pore interface) in the test model of the analysis.

Scales	Treatments	Porosity		Soil-pore interface		Connectivity	
		p-value	Coefficient *β*	p-value	Coefficient *β*	p-value	Coefficient *β*
Macroscale 3D	*Pseudomonas* inoculated in soil with aggregates sizes 1-2 mm	0.009	-1.640	0.007	-0.170	0.039	-0.548
	Pseudomonas inoculated in soil with aggregate sizes 2-4 mm	0.001	3.061	0.000	0.339	0.000	2.583

Figures

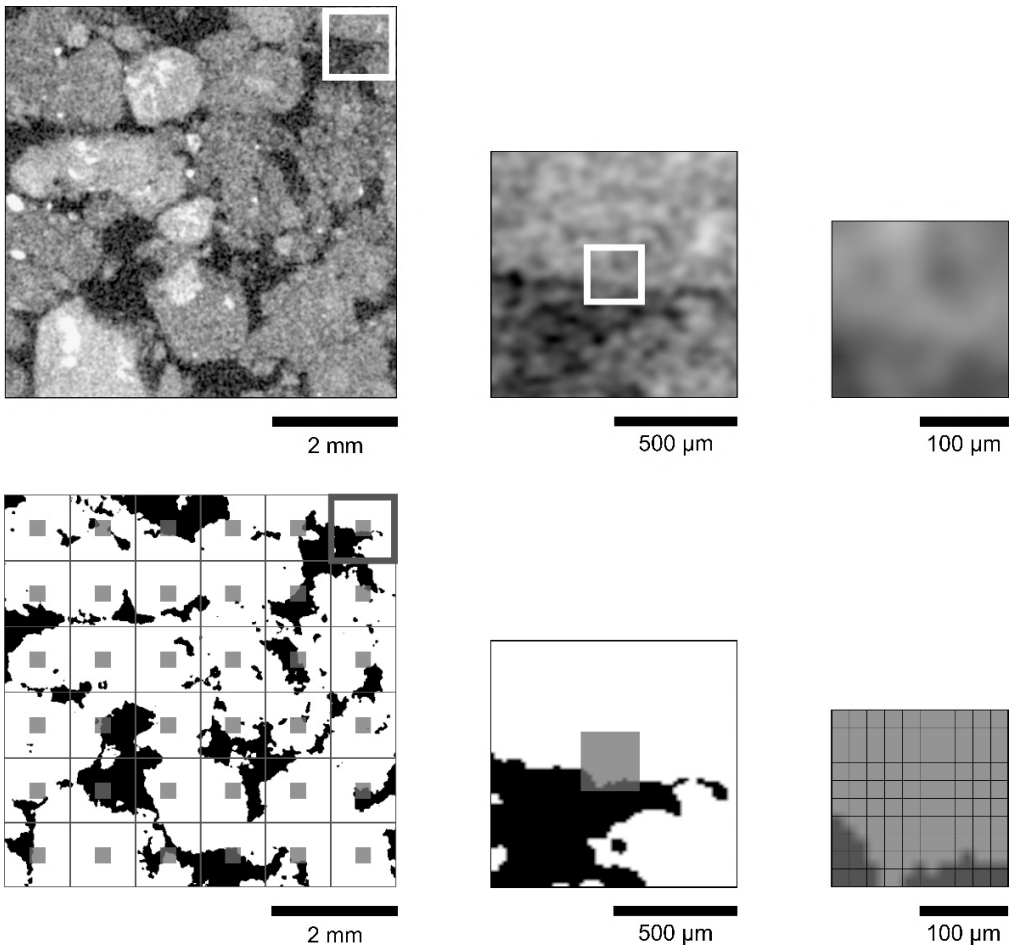

Fig. 1

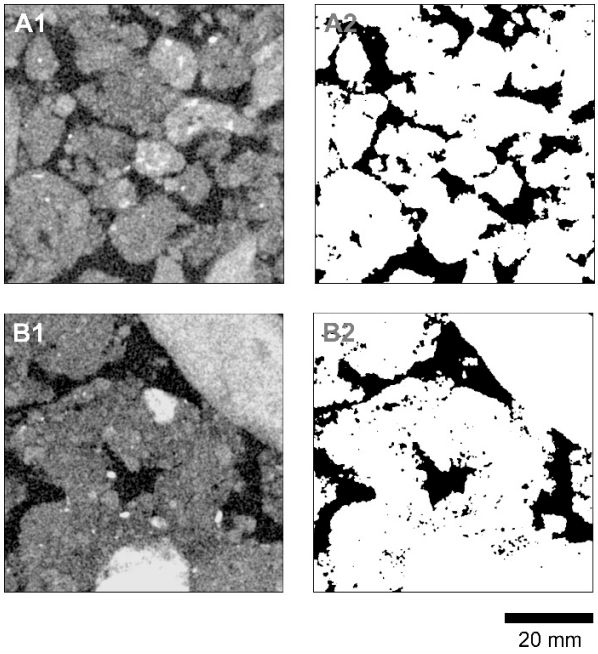

Fig.2

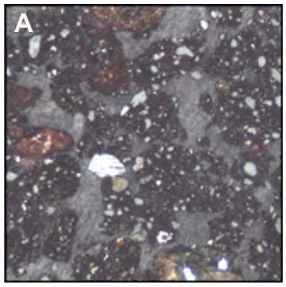

350	325	150	100	50	300
325	175	225	50	325	225
25	350	125	250	325	450
350	50	150	800	325	375
700	525	350	200	175	75
300	525	125	250	200	325

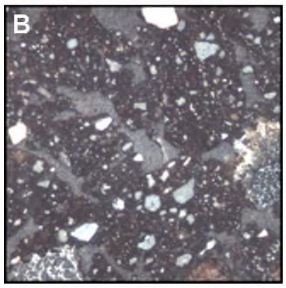

425	475	275	650	175	0
350	425	450	175	75	125
325	350	525	350	250	50
300	250	450	275	175	150
625	300	175	425	325	300
200	225	275	475	400	375

Fig.3

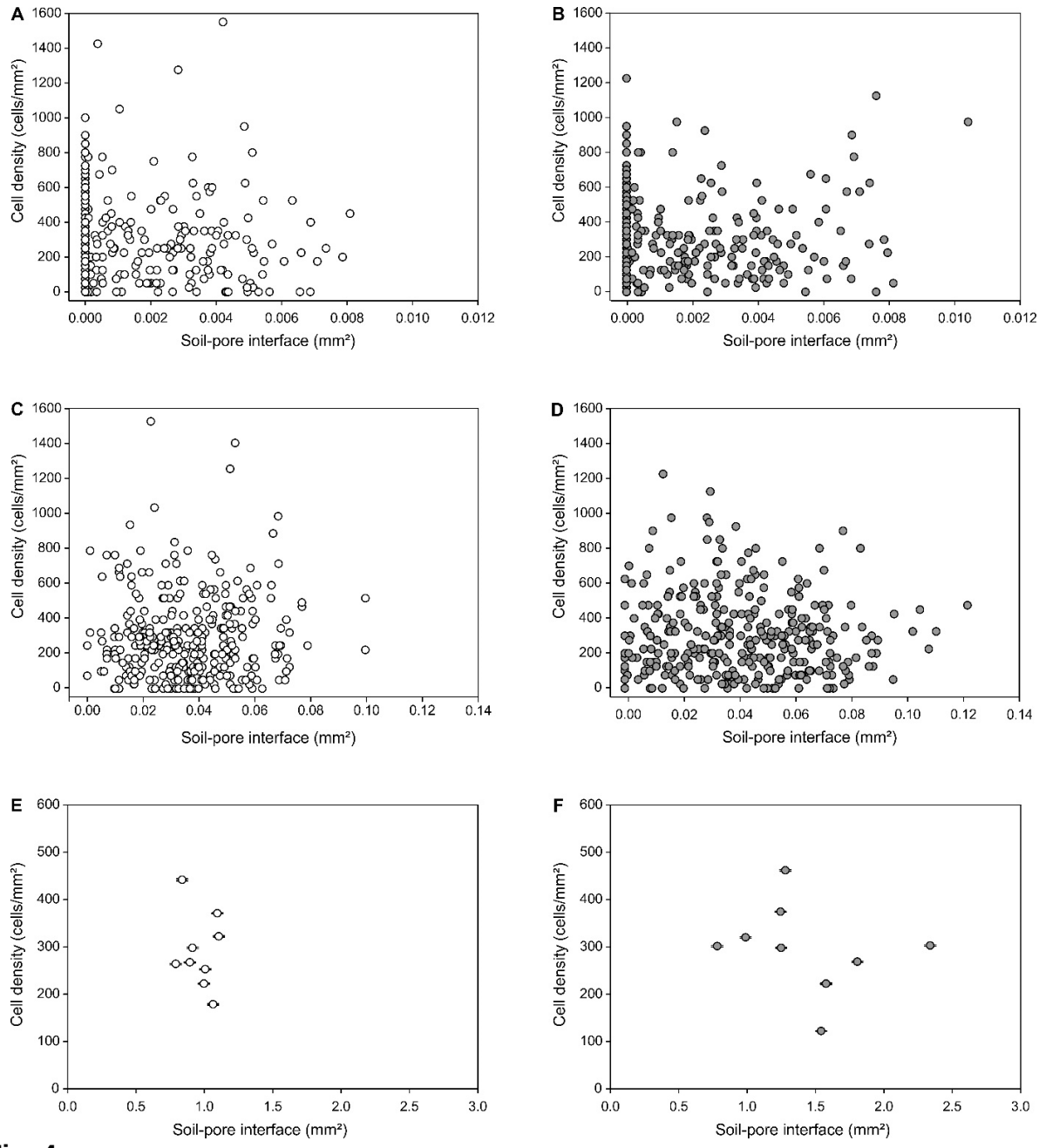

Fig .4

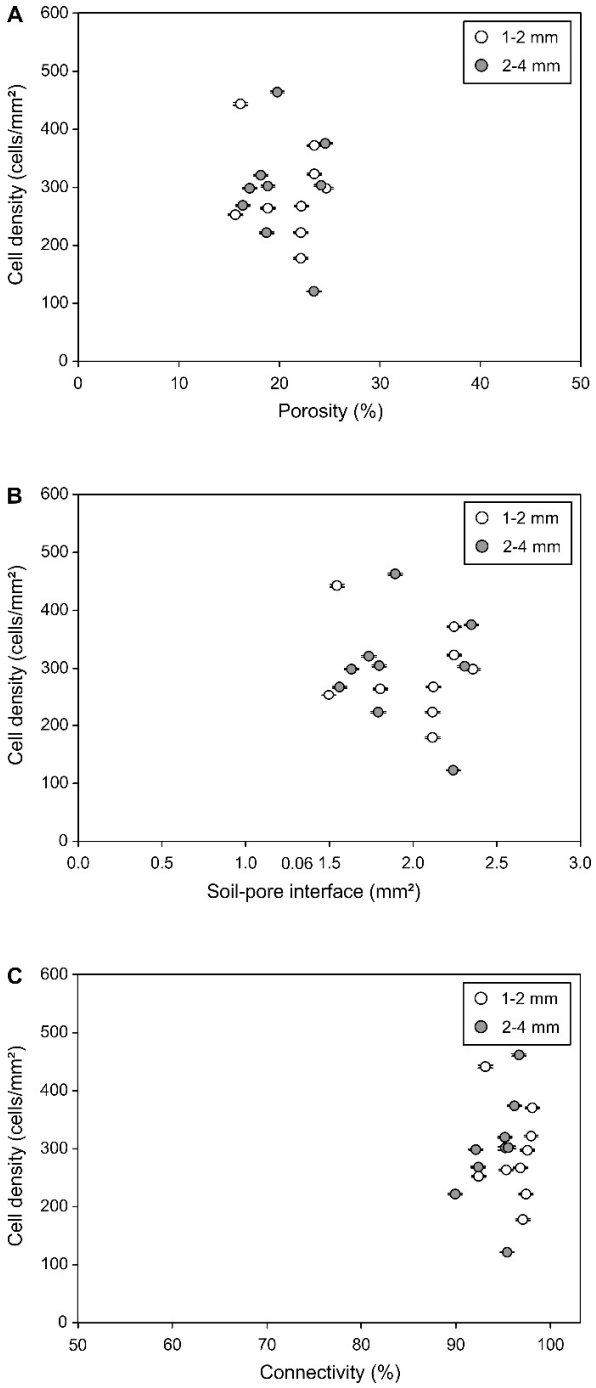
A
B
C
1-2 mm
2-4 mm
Cell density (cells/mm²)
Porosity (%)
Soil-pore interface (mm²)
Connectivity (%)
0.06

Fig .5

Combination of techniques to quantify the distribution of bacteria in their soil microhabitats at different spatial scales

A. Juyal[a, b], W. Otten[a, c], R. Falconer[a], P., S. Hapca[a, d], H. Schmidt[e], P. Baveye[f], T. Eickhorst[b *]

[a] School of Science Engineering and Technology, Abertay University, Dundee, UK

[b] University of Bremen, Bremen, Germany.

[c] School of Water, Energy and Environment, Cranfield University, Cranfield, UK

[d] School of Medicine, University of Dundee, Dundee, UK

[e] Department of Microbiology and Ecosystem Science, University of Vienna, Vienna, Austria

[f] AgroParisTech, Université Paris-Saclay, Thiverval-Grignon, France

* eickhorst@uni-bremen.de

Supplementary information

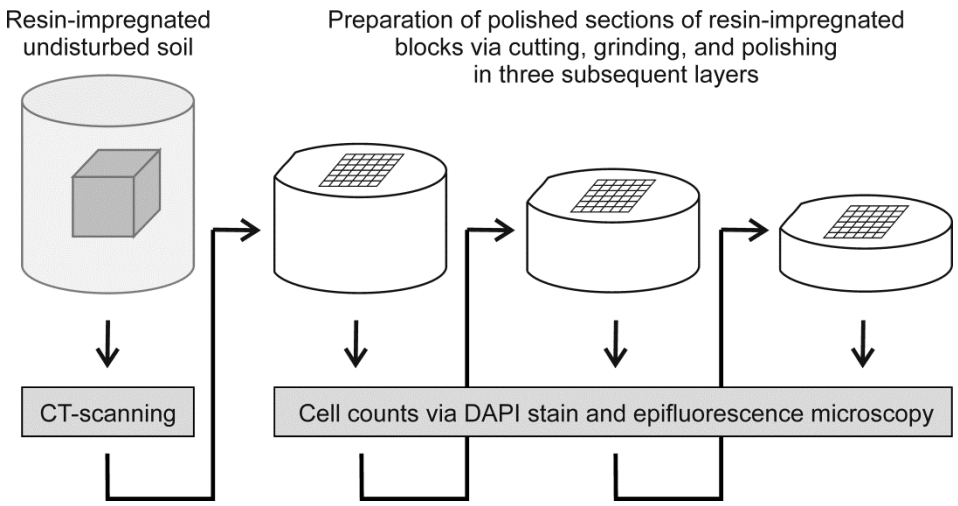

SI Fig. S1 Preparation of three polished sections (layers) from an impregnated soil sample after CT-scanning. The distance between each layer was 2.5 mm. The frames in the diagram represent the counting area (e.g. 5.2 × 5.2 mm).

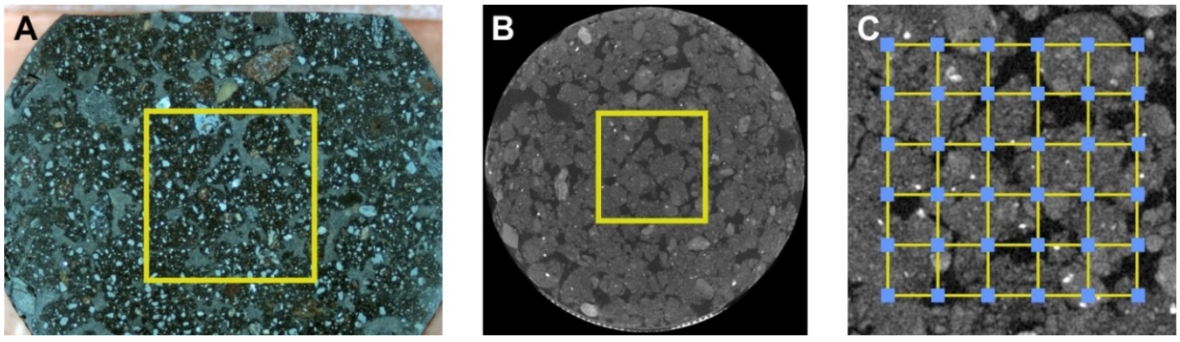

SI Fig. S2 Alignment of stereomicroscope image (A) with CT scanned image (B). Yellow frame represents the area of interest where bacteria were counted. The blue frame (C) represents each counting spot of size 0.2 × 0.2 mm. The distance between each spot was set to 1 mm.

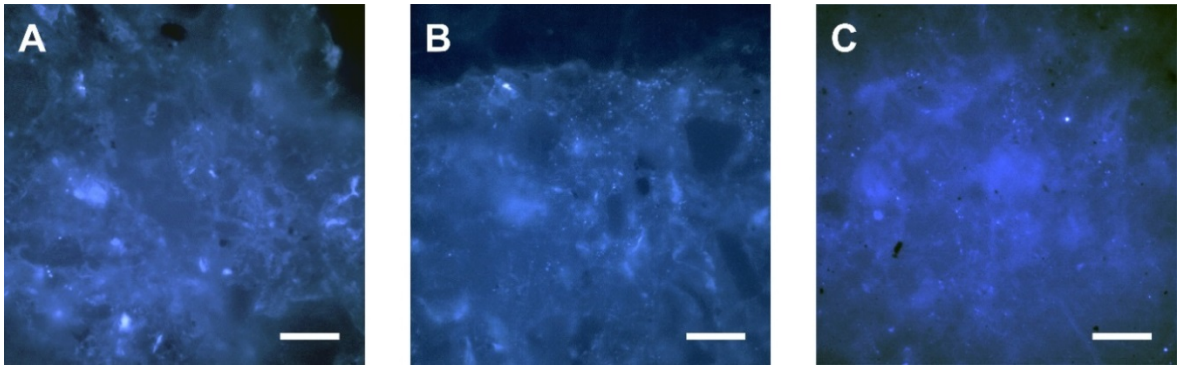

SI Fig. S3 Microscopic images of polished soil sections showing DAPI-stained *Pseudomonas fluorescens* cells under UV excitation filter. Micrographs show the distribution of Pseudomonas cells in the soil matrix (A), soil-pore-interface (B), and aggregate surface (C). Scale bar: 20 µm.

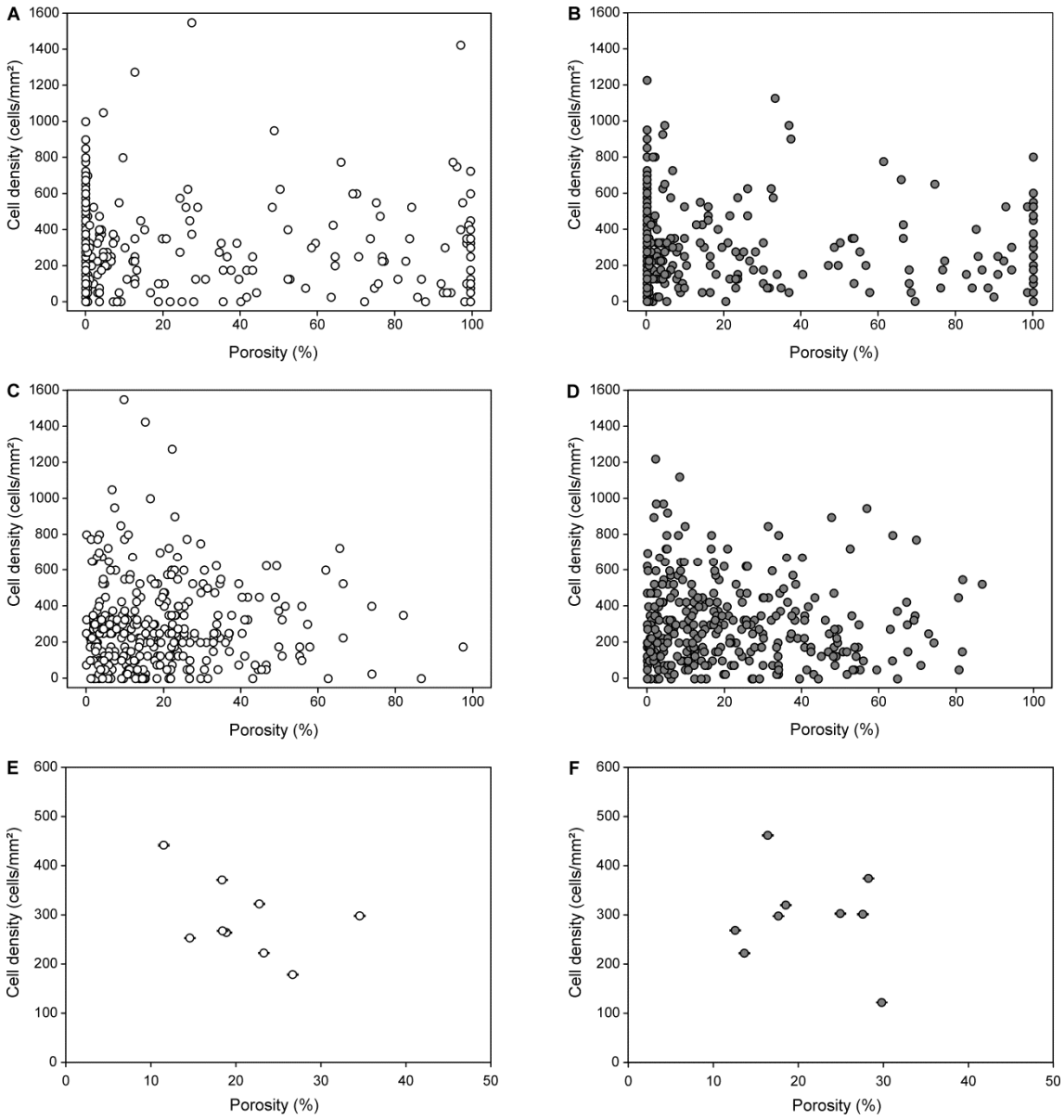

SI Fig. S4 Relationship between bacteria cell density and soil porosity at microscale (A, B), mesoscale (C, D) and macroscale (E, F) in 2D in soil with aggregates of size 1-2 mm (left column; A, C, E) and 2-4 mm (right column; B, D, F). Data points in the graph represent individual counting spots in analyzed layers of each replicate per treatment (microscale and mesoscale) and means of each layer and replicate per treatment (macroscale; ±SE, *n*=3).

SI S5: Test of cell removal during sample preparation

Methodology

In order to test for cell losses during the procedures of fixation, washing, and dehydration, a set of five additional microcosms (1-2 mm aggregate size) has been packed and incubated (see main text). These microcosms were fixed, washed, and dehydrated as described in the Materials and Methods. During this procedure, each microcosm was placed in individual glass beakers to quantify the cell losses per individual microcosm. After fixation, washing in MQ distilled water, and dehydration in 50% (v/v) acetone-water solution the respective solutions were sampled after each step (5 mL each) and transferred on polycarbonate filters (0.2 µm, Millipore). Small pieces were cut from these filters, amended with DAPI stain (Vectashield H-1200, Vector Laboratories, USA) and observed under a fluorescence microscope (see main text). Microbial cells in the tested solutions were enumerated as cells per mL solution and resulting numbers were extrapolated to cells per g soil by using the soil weight of each microcosm. Filters containing the pure solutions for each treatment served as control. An additional set of microcosms packed with non-autoclaved soil aggregates (1-2 mm) has been prepared to test for cell losses of the native soil microorganisms.

Results

Extrapolated cell numbers counted after fixation, washing, and dehydration in the respective solutions are presented in Fig. A4. Cell losses were highest after the first treatment of fixation resulting in $7.9 \times 10^5 \pm 9.4 \times 10^4$ cells per g soil for microcosms inoculated with *Pseudomonas fluorescens* and $1.4 \times 10^4 \pm 2.0 \times 10^3$ cells per g soil for microcosms containing native soil microorganisms. Cell losses decreased in the subsequent treatments of washing ($2.6 \times 10^5 \pm 3.3 \times 10^4$ cells per g soil and $4.3 \times 10^3 \pm 1.4 \times 10^3$ cells per g soil) and dehydration ($1.6 \times 10^5 \pm 4.8 \times 10^4$ cells per g soil and $9.3 \times 10^2 \pm 5.9 \times 10^2$ cells per g soil) for *Pseudomonas fluorescens* and native soil microorganisms respectively.

In order to evaluate the effect of cell losses during sample preparation the proportion has been estimated based on the total number of cells in the two tested types of soil microcosms (*Pseudomonas fluorescens*: $6.3 \times 10^7 \pm 5.1 \times 10^6$; native soil microorganisms: $1.4 \times 10^8 \pm 1.3 \times 10^7$). For soil microcosms inoculated with *Pseudomonas fluorescens* relative cell losses ranged from -1.26% after fixation to -0.25% after dehydration (Fig. A5a). For soil microcosms with non-autoclaved soil relative cell losses were approx.. 100 times lower ranging from -0.01% after fixation down to -0.001% after dehydration (Fig. A5b).

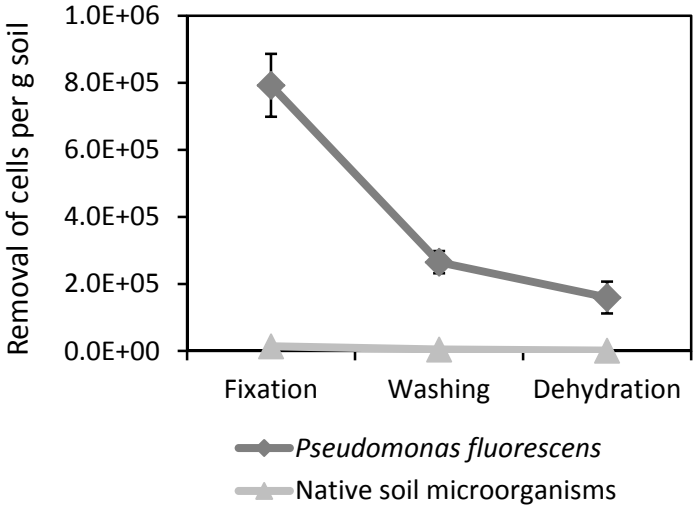

Fig. S5 Removal of microbial cells after the treatments of fixation, washing, and dehydration from packed soil aggregates (1-2 mm) inoculated with *Pseudomonas fluorescens* and non-autoclaved packed soil aggregates (1-2 mm; native soil microorganisms). Cell numbers were enumerated in the respective solutions and extrapolated to g soil. Error bars: standard error (n = 5).

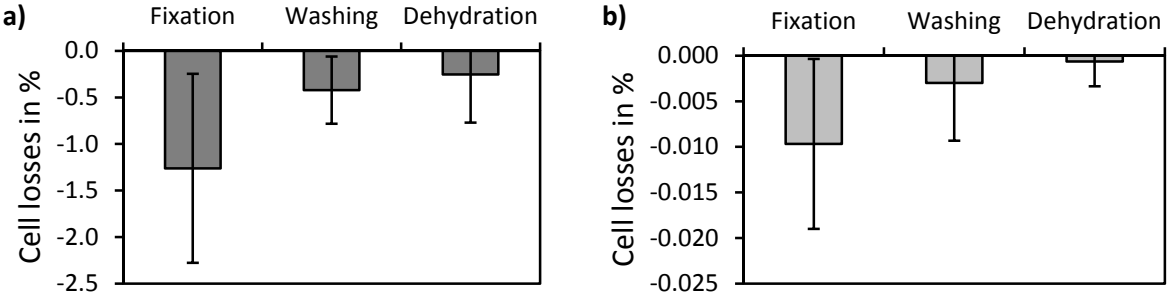

Fig. S6 Losses of cells given as percentage based on the total number of cells in the two tested types of soil microcosms. **(a)** Packed soil aggregates (1-2 mm) inoculated with *Pseudomonas fluorescens*; total cell counts $6.3 \times 10^7 \pm 5.1 \times 10^6$ **(b)** Packed non-autoclaved soil aggregates (1-2 mm) representing the native soil microorganisms; total cell counts $1.4 \times 10^8 \pm 1.3 \times 10^7$. Error bars: standard error (n = 5).